Increasing contribution of evaporative demand to future intensified drought across global drylands

Xiaojing Yu[1,2], Lixia Zhang[1], Tianjun Zhou[1,2,3], Dan Zhao[1,2], Ziming Chen[1,2]

[1]LASG, Institute of Atmospheric Physics, Chinese Academy of Sciences, Beijing, China

[2]University of the Chinese Academy of Sciences, Beijing, China

To be submitted to Earth's Future

* Corresponding author: lixiazhang@mail.iap.ac.cn

ABSTRACT

Drylands face more threat from droughts under global warming. It remains insufficient in quantifying the roles of potential evapotranpiration (PET) and precipitation (P) to drought changes in a warming climate. Thus, we quantified the relative contributions of PET and P and projected their future changes across global drylands under four scenarios from Phase Six of the Coupled Model Intercomparison Project (CMIP6) models. In the 21st century, the multimodel medians of hydroclimatic fields indicate relatively consistent trend patterns, showing a drying over most of global drylands except for East Asia, Middle East, Sahel and South Asia drylands. The standardized precipitation evapotranspiration index (SPEI) presents a robust and ubiquitous drying with scenario-dependent magnitudes. The fractional contributions of PET and P to the present-day drought changes are estimated to be approximately equal (~50%). For the near- and mid-term projections, PET (P) contributes ~58% (42%) and ~61% (~39%), respectively. In the long-term, the fractional contribution of PET (P) reaches ~65% (~35%), ~72% (28%), ~80% (~20%), ~85% (~15%) under four different scenarios, respectively. Furthermore, PET contributes more significantly in the North Hemisphere than in the South Hemisphere, particularly over the Mediterranean, central and East Asian drylands. Drought conditions tend to be relatively stable under low scenarios (SSP1-2.6 and SSP2-4.5), while exacerbate continuously under high scenarios (SSP3-7.0 and SSP5-8.5). By the end of 21st century, severe droughts like the present-day 1-in-20-yr events are estimated to become fairly common across global drylands. These results provide further understanding for making policy and adaption strategies for drylands.

Plain Language Summary

Drought is an essential natural hazard and even more damaging over the drought-prone drylands. The hydroclimatic fields present regional discrepancies in the sign of future trend, drying over North America, South America, Mediterranean, central Asia, Southern Africa and Australia drylands, while wetting over East Asia, Middle East, Sahel, and South Asia drylands. Additionally, the standardized precipitation evapotranspiration index (SPEI), comprising the impacts of precipitation and potential evapotranspiration, shows a robust and ubiquitous drying across global drylands. Under different warming levels, the future contributions of the potential evapotranspiration (PET) and precipitation tend to increase and decline with time, respectively. In general, PET contributes more significantly over drylands in the North Hemisphere than in the South Hemisphere, in regards to their nearly equal roles in the 20th century. Basically, projections by CMIP6 models indicate more widespread, intense and frequent droughts across global drylands, which is mainly attributed to the substantially increased PET in a warming climate.

Key points:

- Hydroclimatic fields present a drying over most of global drylands except for East Asia, Middle East, Sahel and South Asia drylands.
- Fractional contribution of PET (precipitation) across global drylands is expected to increase (decrease) with time under different scenarios.
- Severe droughts like the present-day 1-in-20-yr events are estimated to become fairly common across global drylands by the end of 21st century.

1 Introduction

Drought is a slow-onset but damaging hydroclimatic hazard with broad spatio-temporal scales (Gill & Malamud, 2014; Ault, 2020). Severe droughts have cascading impacts not only on environmental systems (Vicente-Serrano et al., 2020), but also on socioeconomic development (Liu & Chen, 2021). Drylands, drought-prone regions characterized by scarce precipitation (P) and high evaporative demand [measured by potential evapotranspiration (PET)], occupy ~41% of global terrestrial land (White & Nackoney, 2003) and are home to ~38% of the world's total population [United Nations Development Programme (UNDP), 2014]. For their vulnerable ecosystems and low societal resilience, drylands face more threat than humid regions once hit by droughts, such as water and food deficits, population migrations and international disputes (Mannava et al., 2013; Barlow et al., 2016; Ault, 2020; Fragaszy et al., 2020). Therefore, knowledge of the risks and severity for future droughts is a prerequisite to make policies and adaption strategies in drylands.

Global widespread aridity has increased substantially since the 1980s in terms of both hydrological fields (i.e., P, runoff, and soil moisture) and drought indices, although with somewhat regional inhomogeneity (Dai, 2013, 2021; Trenberth et al., 2014; Dai & Zhao, 2017). The key factor exacerbating land drying is attributed to the land-atmosphere feedbacks in response to greenhouse warming (Sherwood & Fu, 2014; Berg et al., 2016). Legions of recent studies have projected robust increase in intensity, frequency, and duration of droughts in a warmer climate (Lehner et al., 2017; Zhou et al., 2019; Hari et al., 2020; Takeshima et al., 2020; Ukkola et al., 2020), which is dominated by the warming-induced PET (Cook et al., 2014; Fu & Feng, 2014; Scheff & Frierson, 2015; Milly & Dunne, 2016; Zhao & Dai, 2017; Dai et al., 2018; Spinoni et al., 2020). Some researchers have assessed the relative contributions of P and PET to the magnitude and extent of global terrestrial aridity (Cook et al.,

2014; Scheff & Frierson, 2015). However, little has been done to reveal how their contributions will change in a warming climate, especially in those regions where changes in P and PET offset each other.

Under climate change, drylands experienced a more evident warming in the last century, accounting for more than half of the continental warming (Huang et al., 2012; Ji et al., 2014). For the intensified land-atmosphere feedbacks, drylands response more dramatically to climate change (Huang et al., 2017a, 2017b; Wei et al., 2019), such as accelerated expansion (Feng & Fu, 2013; Huang et al., 2015), higher risks of degradation and desertification (Yao et al., 2020; Huang et al., 2020; Burrell et al., 2020). Relatively few studies have addressed the future drought changes across global drylands (Schlaepfer et al., 2017; Miao et al., 2020). Therefore, we focus on the two questions in this study: (1) To what extent, P and PET contribute to future drought changes throughout the global drylands? (2) How severe will droughts impact drylands in a warming climate?

In the following, Section 2 describes the data and methods used in this study. Subsequently, detailed results are illustrated in Section 3. To the end, we summarize and discuss the results in Section 4.

2 Data and methods

2.1 Observation and definition of drylands

We use the Climatic Research Unit gridded Time Series Version 4.03 (CRU TS v.4.03) with a spacial resolution of 0.5° latitude × 0.5° longitude (Harris et al., 2020), which is available at http://data.ceda.ac.uk/badc/cru/data/cru_ts/cru_ts_4.03. Two variables including the observed P and derived PET during 1960–2018 are applied to define the global drylands.

Drylands are generally defined by the aridity index (AI), which is the ratio of annual P to PET (Middleton & Thomas, 1992; Hulme, 1996; Feng & Fu, 2013; Huang et al., 2015). Here global drylands are measured as regions with AI less than 0.65 for the 1960–2018 climatology, in line with the previous studies (Feng & Fu, 2013; Huang et al., 2015).

2.2 Standardized precipitation evapotranspiration index (SPEI)

In this study, drought is quantified by the standardized precipitation evapotranspiration index (SPEI, Vicente-Serrano et al., 2010). This index considers both P and evaporative demand, and can be calculated on different time scales to characterize different types of droughts (Vicente-Serrano et al., 2012). Here the 12-month SPEI is applied to measure the long-lasting drought for its detrimental impacts on society and ecology. Droughts are then divided into mild (-0.5≤SPEI<-1.0), moderate (-1.0≤SPEI<-1.5), severe (-1.5≤SPEI<-2.0) and extreme(SPEI≤-2.0) droughts (Vicente-Serrano et al., 2010). Among numerous ways to estimate PET (Xie & Wang, 2020), we use the Penman–Monteith method, based on surface moisture and energy balance considerations, recommended by the Food and Agricultural Organization (FAO) of the United Nations (Penman 1948; Monteith 1965; Zotarelli et al., 2013).

2.3 CMIP6 models

We use model outputs from the Coupled Model Intercomparison Project Phase 6 (CMIP6, https://esgf-node.llnl.gov/search/cmip6/), including historical simulations and projections under four combined scenarios of the Shared Socioeconomic Pathways (SSP) and the Representative Concentration Pathways (RCP), i.e., SSP1-2.6, SSP2-4.5, SSP3-7.0, SSP5-8.5 scenarios (Eyring et al., 2016; O'Neil et al., 2016, 2017). Given the data availability for calculating PET, monthly variables from one realization of 13 CMIP6 models are selected (Table.1). All outputs are regridded to 1.5° latitude × 1.5° longitude via bilinear interpolation. Variables including P,

evapotranspiration (E), surface soil moisture content (SM) are applied to analyze the future changes for hydroclimate. SM is unavailable from INM-CM4-8 and INM-CM5-0. Variables, including near surface air temperature, specific humidity, wind, radiation, are applied to estimate PET. Moreover, four specific periods are examined and termed as the present day (1995–2014), near-term (2021–2040), mid-term (2041–2060), and long-term (2051–2100), respectively.

Table 1 Details of CMIP6 models used in this study

No	Model	Institute (Country)	Lat × Lon
1	ACCESS-CM2	Commonweaalth Scientific and Industrial Research Organization and Bureau of Meteorology (Australia)	144×192
2	ACCESS-ESM1-5		145×192
3	BCC-CSM2-MR	Beijing Climate Center (China)	160×320
4	CanESM5	Canadian Centre for Climate Modelling and Analysis (Canada)	64×128
5	FGOALS-f3-L	Institute of Atmospheric Physics, Chinese Academy of Sciences (China)	180 x 360
6	INM-CM4-8	Institute for Numerical Mathematics, Russia	120 x 180
7	INM-CM5-0		
8	IPSL-CM6A-LR	Institute Pierre Simon Laplace (France)	143 x 144
9	MIROC6	Atmosphere and Ocean Research Institute (The University of Tokyo), National Institute for Environmental Studies, and Japan Agency for Marine-Earth Science and Technology (Japan)	128 x 256
10	MIROC-ES2L		64 x 128
11	MPI-ESM1-2-HR	Max Planck Institute for Meteorology (MPI-M)	192 x 384
12	MPI-ESM1-2-LR		96 x 192
13	MRI-ESM2-0	Meteorological Research Institute (Japan)	96 x 192

2.4 Analysis methods

In the process of calculating SPEI, the baseline period is set to 1960–1989 because the observed drought area and frequency increase remarkably since the 1990s across

global drylands (Vicente-Serrano et al., 2010; Dai, 2011; Dai & Zhao, 2017). To quantify the relative contributions of PET and P, we calculate four versions of SPEI for 1900–2100 following as Cook et al. (2014). They are termed as SPEI_All, SPEI_PET, SPEI_P and SPEI_Sum, respectively. First, we calculate SPEI using P and estimated PET from model outputs, which incorporates changes in both P and PET, referred as SPEI_All. Secondly, we isolate the impact of PET (P) by detrending monthly P (PET) during 1990–2100 and setting the mean to be equal to the 1960–1989 climatology. Then, SPEI_PET (SPEI_P), only considering the impact of PET (P), is calculated by using PET (P) and the detrended P (PET). Finally, SPEI_Sum, the sum of SPEI_PET and SPEI_P, is calculated to compare with SPEI_All. SPEI_Sum is higher than SPEI_All because P and PET are not completely independent, in accord with Cook et al. (2014). Overall, SPEI_Sum and SPEI_All are consistent enough to be used to investigate the respective impact of PET and P.

The relative contributions of P and PET to SPEI are ultimately expressed as the following formula:

$$\mathrm{SPEI\_Sum} = \mathrm{SPEI\_PET} + \mathrm{SPEI\_P} \quad (1)$$

$$\Delta\mathrm{SPEI\_Sum} = \Delta\mathrm{SPEI\_PET} + \Delta\mathrm{SPEI\_P} \quad (2)$$

$$\mathrm{Perc(PET)} = \Delta\mathrm{SPEI\_PET}/\Delta\mathrm{SPEI\_Sum} \quad (3)$$

$$\mathrm{Perc(P)} = \Delta\mathrm{SPEI\_P}/\Delta\mathrm{SPEI\_Sum} \quad (4)$$

where Δ indicates SPEI changes relative to the 1960–1989 baseline. Perc(PET) and Perc(P) are the contribution of changes in PET and P to changes in SPEI, respectively.

3 Results

3.1 Future changes in hydroclimate

We first analyze the projected changes of hydroclimatic fields area-averaged over

global drylands (Figure 1). Besides P and E, we also examine the future changes of surface water availability, namely precipitation minus evapotranspiration (P-E), and surface soil moisture (SM) for their indication in agricultural and hydrological droughts (Zhao & Dai, 2015; Cook et al., 2020; Zhou et al., 2021). P, E and P-E tend to increase consistently, more robust under the two high scenarios than the two low scenarios. Nevertheless, SM presents a relatively slight decreasing with much larger model uncertainties. By the end of the 21st century, the multi-model median projects an increase of ~4, 5, 8 and 10% for P, ~4, 5, 6 and 9 % for E, ~2, 4, 10, and 20% for P-E, whereas a decline of ~1, 1, 1.5 and 2% for SM under SSP1-2.6, SSP2-4.5, SSP3-7.0 and SSP5-8.5 scenarios, respectively, relative to the 1960–1989 climatology.

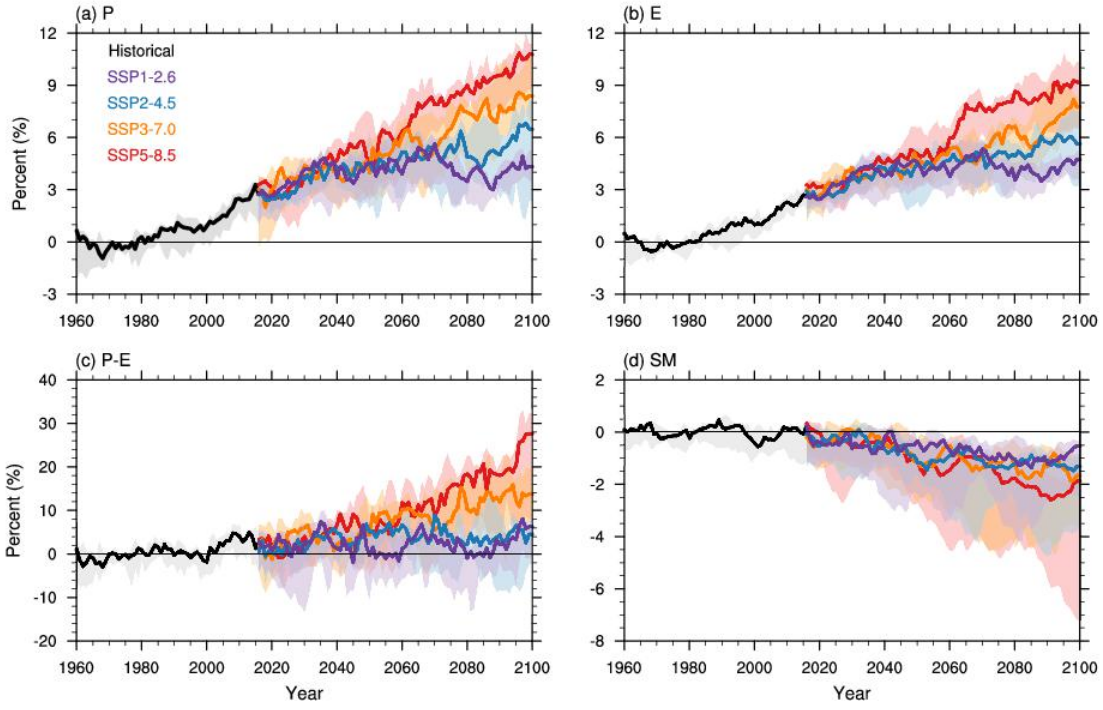

Figure 1. 10-year running mean of the projected changes (unit: %) in annual mean precipitation (P, a), evapotranspiration (E, b), precipitation minus evapotranspiration (P-E, c), and surface soil moisture (SM, d) across global drylands during 1960–2100, relative to 1960-1989 climatology. Historical (black), SSP1-2.6 (purple), SSP2-4.5 (blue), SSP3-7.0 (orange), and SSP5-8.5 (red) simulations are shown in median (lines) and interquartile ranges (shade).

Then we elaborate the spatial pattern of hydroclimatic changes over global drylands. Figure 2 shows distributions of linear trends for annual P and E across global drylands during 2015–2100 under the four different scenarios. On the whole, P and E present consistent features in spatial patterns and scenario-dependent magnitudes. Under each SSP scenario, P and E tend to increase over northwestern America, central and East Asia, and Sahel drylands, while decrease over southwestern America, South America, Mediterranean, Southern Africa, and the majority of Australia drylands. In addition, the magnitudes of changes and agreements in the trend sign are intensifying with warming level. Estimated from the area-averaged multimodel medians and interquartile ranges, P (E) presents an overall increasing of 0.3 (-4.7, 2.8) [0.7(-3.3, 3.0)], 4.8 (0.8, 7.5) [5.1 (1.8, 7.1)], 11.6 (8.3, 16.0) [11.6 (8.5, 15.7)], and 14.1 (9.0, 29.5) [13.6 (9.6, 26.6)] %/100yr across global drylands under SSP1-2.6, SSP2-4.5, SSP3-7.0, and SSP5-8.5 scenarios, respectively.

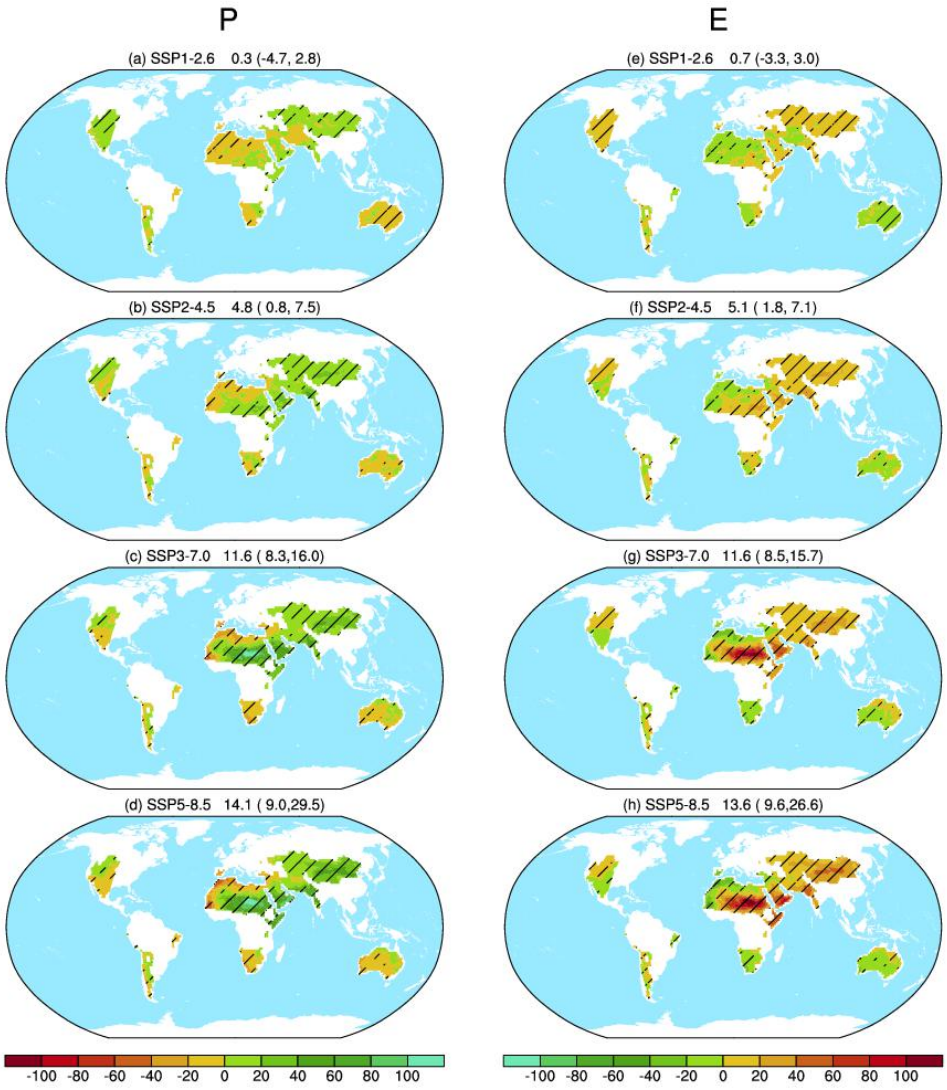

Figure 2. Multimodel medians of future linear trends (unit: %/100yr) for annual precipitation (P, a–d) and evapotranspiration (E, e–h) over global drylands during 2015–2100 under SSP1-2.6 (a, e), SSP2-4.5 (b, f), SSP3-7.0 (c, g), and SSP5-8.5 (d, h) scenarios, respectively. Slant hatchings denote where 9/13 of the CMIP6 models agree in the sign of trend. The numbers in the top of each plot are the multimodel medians and interquartile ranges of area-averaged trend across global drylands, respectively.

Figure 3 provides distributions of linear trend for annual P-E and SM over global drylands during 2015–2100 under the four different scenarios. Clearly, P-E and SM also present roughly consistent patterns and scenario-dependent magnitudes, in accord with P and E. In the 21st century, P-E and SM tend to get drying over most of the global drylands, including North America, South America, Mediterranean, central

Asia, Southern Africa and Australia drylands, where P decreases or increases indistinctively. Conversely, obvious wetting can be seen over the regions where P increases robustly, including the arid East Asia, Sahel, Middle East and South Asia. Note that P-E shows more localized and divergent patterns, especially over complex terrains. Area-averaged across global drylands, P-E shows a wetting of 1.5 (-4.6, 10.7), 9.7 (-14.2, 61.5), 15.8 (-15.0, 103.7) and 26.6 (-92.9, 52.0) %/100yr, whereas SM presents a drying of -0.9 (-3.0, 0.1), -1.5 (-3.3, -0.3), -1.5 (-3.5, -0.8) and -1.9 (-4.6, -0.6) %/100yr under the four different scenarios, respectively. It seems somewhat paradoxical that the area-averaged P-E and SM are opposite in the future changes (Figure 1c-d, Figure 3). Moreover, the inter-model uncertainties of P-E and SM are also larger than P and E. These results are in line with previous studies (Dai et al., 2018; Cook et al., 2020), which is mainly because water availability and SM are affected by different temperature-sensitive factors (such as snow, vegetation and E) and their negative feedbacks (Zhang et al., 2014; Mankin et al., 2019; Zhou et al., 2021).

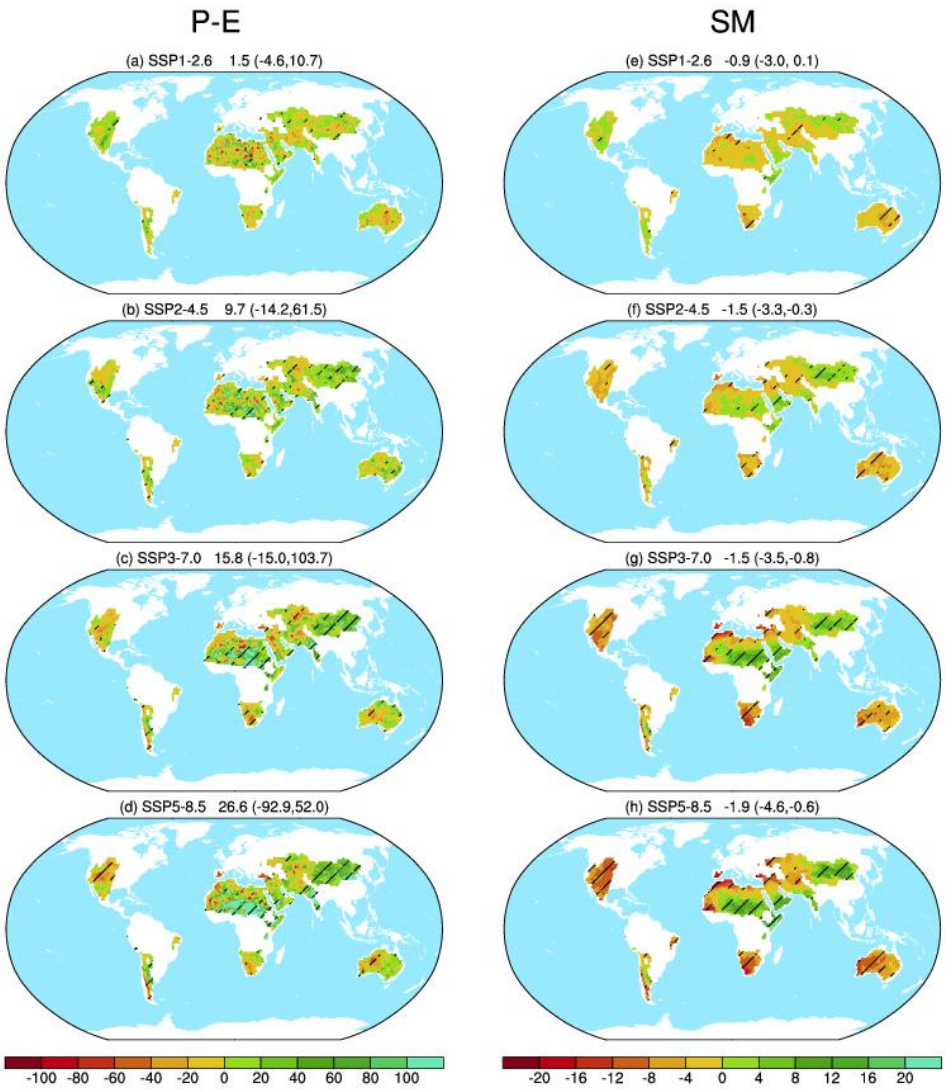

Figure 3. Same as Figure 2, but for precipitation minus evapotranspiration (P-E, a–d) and surface soil moisture (SM, e–h). Slant hatchings denote where 8/11 for SM (9/13 for P-E) of the CMIP6 models agree in the sign of trend.

3.2 Relative contributions of PET and P to drought changes

In this section, we use SPEI to investigate drought changes and roles of PET and P to SPEI changes in global drylands in the future projection. Before quantifying the contributions of PET and P, it is necessary to verify the reliability of SPEI for specific calculations. We first examine future changes in drought conditions via SPEI_All, SPEI_Sum, SPEI_PET and SPEI_P (Figure 4). The drought indices comprising the

change of PET, i.e., SPEI_All, SPEI_Sum, SPEI_PET, tend to decline consistently in the 21st century, indicating an exacerbating drying condition because of enhanced PET. Estimated from the multimodel medians, the three indices decrease from ~0.0 in the 20th century to ~ -0.5, -1.0, -1.3 and -1.5 in the end of 21st century, under SSP1-2.6, SSP2-4.5, SSP3-7.0, and SSP5-8.5 scenarios, respectively. The scenario inconsistencies are also becoming more evident with time, particularly in the second half of the 21st century. On the contrary, SPEI_P presents a very slight wetting with small scenario uncertainties.

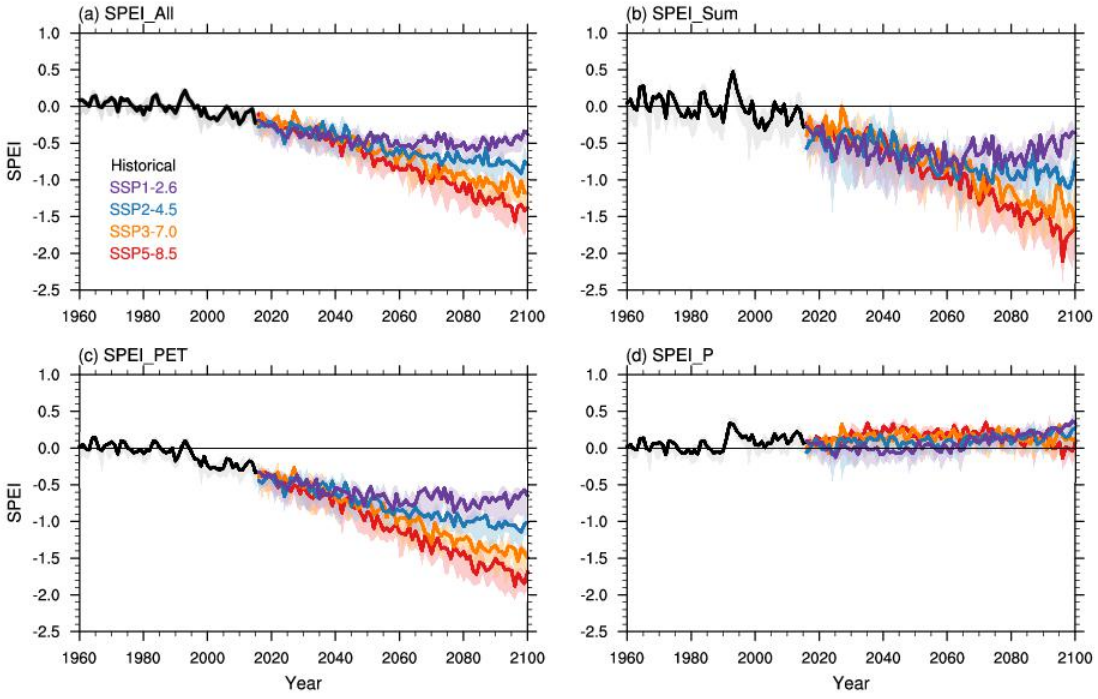

Figure 4. Projected changes in annual mean (a) SPEI_All, (b) SPEI_Sum (c) SPEI_PET and (d) SPEI_P across global drylands during 1960–2100. Historical (black), SSP1-2.6 (purple), SSP2-4.5 (blue), SSP3-7.0 (orange), and SSP5-8.5 (red) simulations are shown in median (lines) and interquartile ranges (shade).

We further illustrate distributions of linear trend for annual SPEI_All (Figure 5) and SPEI for the three specific calculations (Figure 6) over global drylands during 2015–2100 under the four scenarios. Unlike the above hydroclimatic fields, a widespread declining of SPEI_All can be found throughout global drylands under the

four scenarios (Figure 5), which is highly consistent with the substantial increasing of PET (Figures not shown). The area-averaged SPEI_All shows a drying of -0.2 (-0.4, -0.2), -0.7 (-0.8, -0.6), -1.1 (-1.4, -1.0) and -1.4 (-1.7, -1.4) /100yr under the four scenarios, respectively.

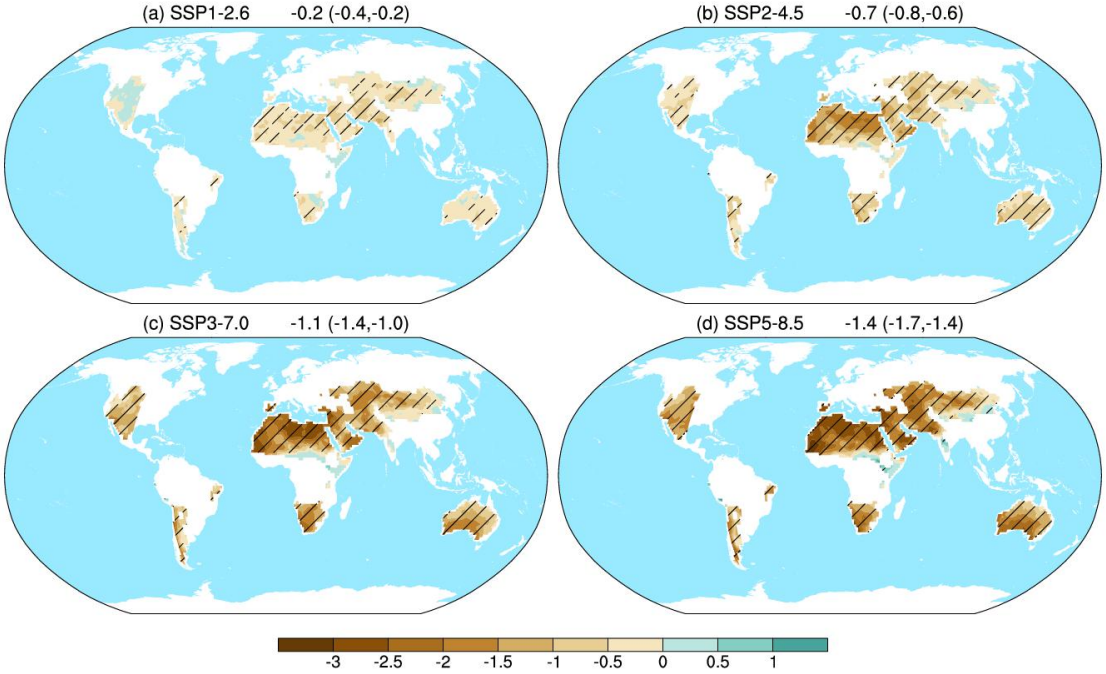

Figure 5. Multimodel medians of future linear trends for SPEI_All (unit: /100yr) over global drylands during 2015–2100 under SSP1-2.6 (a), SSP2-4.5 (b), SSP3-7.0 (c), and SSP5-8.5 (d) scenarios, respectively. Slant hatchings denote where 9/13 of the CMIP6 models agree in the sign of trend.

As illustrated in Figure 6 a–d, widespread drying occurs at a rate of 0.0 (-0.3, 0.1), -0.6 (-0.9, -0.5), -1.2 (-1.6, -1.1), and -1.6 (-2.0, -1.6) /100yr throughout global drylands under the four different scenarios, respectively, estimated by the area-averaged multimodel medians and interquartile ranges. Clearly, SPEI_Sum is highly consistent with SPEI_All (Figure 5) in the spatial patterns of future drought changes, but changes a little more remarkably with relatively larger uncertainties related to scenario and model. This agrees with the validation results that the slope between SPEI_Sum and SPEI_All is slightly larger than 1.0. As for SPEI_PET

(Figure 6e–h), a more widespread and robust drying can be seen across the global drylands, at a rate of -0.3 (-0.6, -0.3), -0.8 (-1.1, -0.8), -1.4 (-1.7, -1.3), -1.7 (-2.0, -1.6) /100yr under the four different scenarios, respectively. SPEI_P (Figure 6 i–l) presents an overall wetting under SSP1-2.6 and SSP2-4.5 scenarios, and tends to diverse under SSP3-3.7 and SSP5-8.5 scenarios, at an area-averaged rate of 0.3 (0.2, 0.4), 0.3 (0.0, 0.3), 0.2 (0.0, 0.3) and 0.2 (-0.1, 0.2) /100yr, respectively. Therefore, the derived SPEI_PET and SPEI_P can reasonably reflect the impacts of PET and P on future drought changes, respectively, and can be used to quantify the contributions of PET and P.

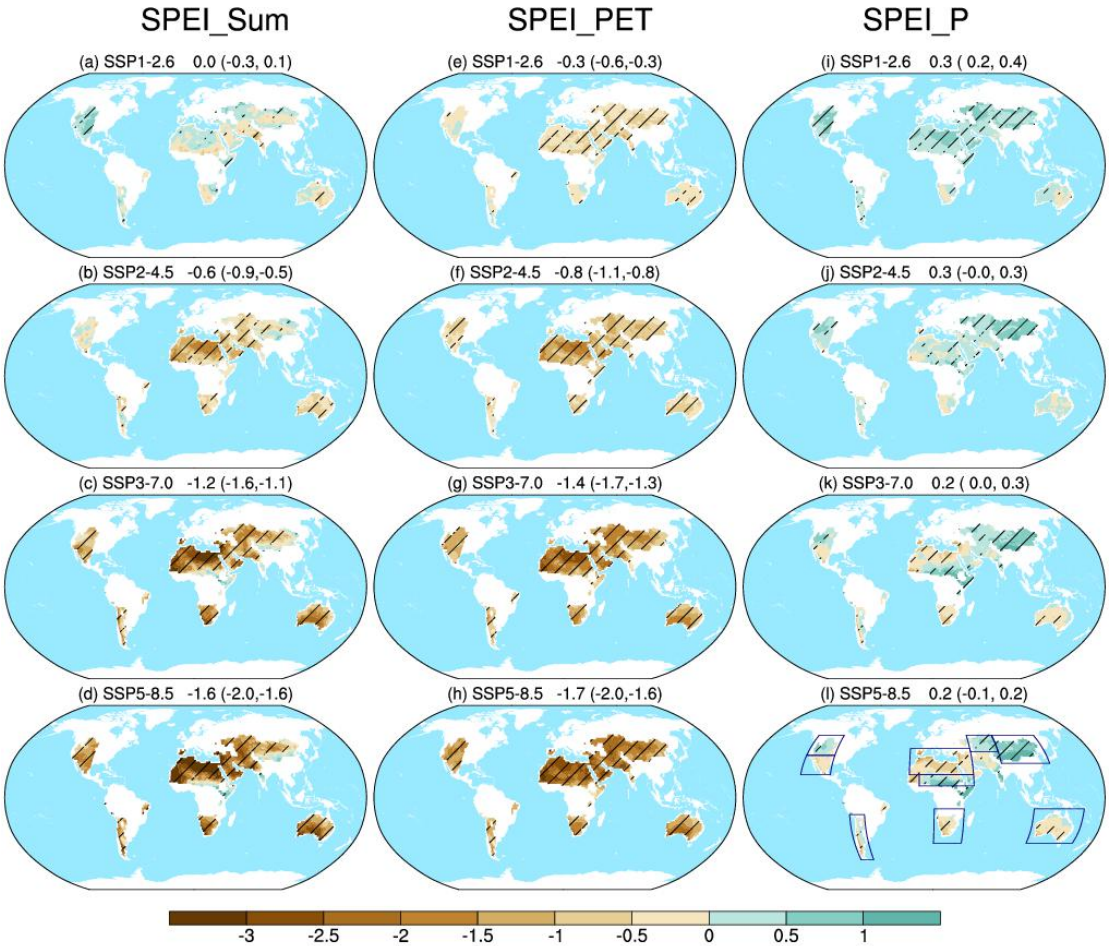

Figure 6. Same as Figure 5, but for SPEI_Sum (a–d), SPEI_PET (e–h) and SPEI_P (i–l). The boxes in (l) denote the nine specific sub-drylands divided by the trend signs of SPEI_P under

SSP3-7.0 and SSP5-8.5 scenarios.

Under SSP3-7.0 and SSP5-8.5 scenarios, SPEI_P shows a wetting over the regions where P increases significantly, including Northwestern America, central and East Asia, and Sahel drylands, while drying over the regions where P decreases or increases slightly, including Southwestern America and the South Hemisphere (Figure 6 k–l). Thus, we divide global drylands into nine sub-drylands (Figure.6 l), and further investigate their area-averaged trends of the four SPEI calculations under the four scenarios (Figure 7). From the perspective of global drylands, SPEI_All, SPEI_Sum and SPEI_PET all see a robust drying, at a rate of -0.3, -0.5 and -0.6 /100yr under SSP1-2.6 scenario, -0.8, -0.8 and -1.0 /100yr under SSP2-4.5 scenario, -1.2, -1.0 and -1.2 /100yr under SSP3-7.0 scenario, -1.5, -1.1 and -1.5 /100yr under SSP5-8.5 scenario, respectively. However, SPEI_P experiences a slight wetting of 0.1, 0.15, 0.2 and 0.3 /100yr under the four scenarios, indicating the future intensifying drought condition dominated by PET can be balanced by P a bit. Regionally, SPEI_All, SPEI_Sum and SPEI_PET still tend to get drying but with different magnitudes among sub-drylands. In particular, the drying rate in the Mediterranean is nearly twice of the mean rate across global drylands. In addition, SPEI_P presents a significantly regional discrepancy, declining slightly over the Mediterranean regions and drylands in the South Hemisphere, while increasing over the other four sub-drylands especially East Asia and Sahel drylands.

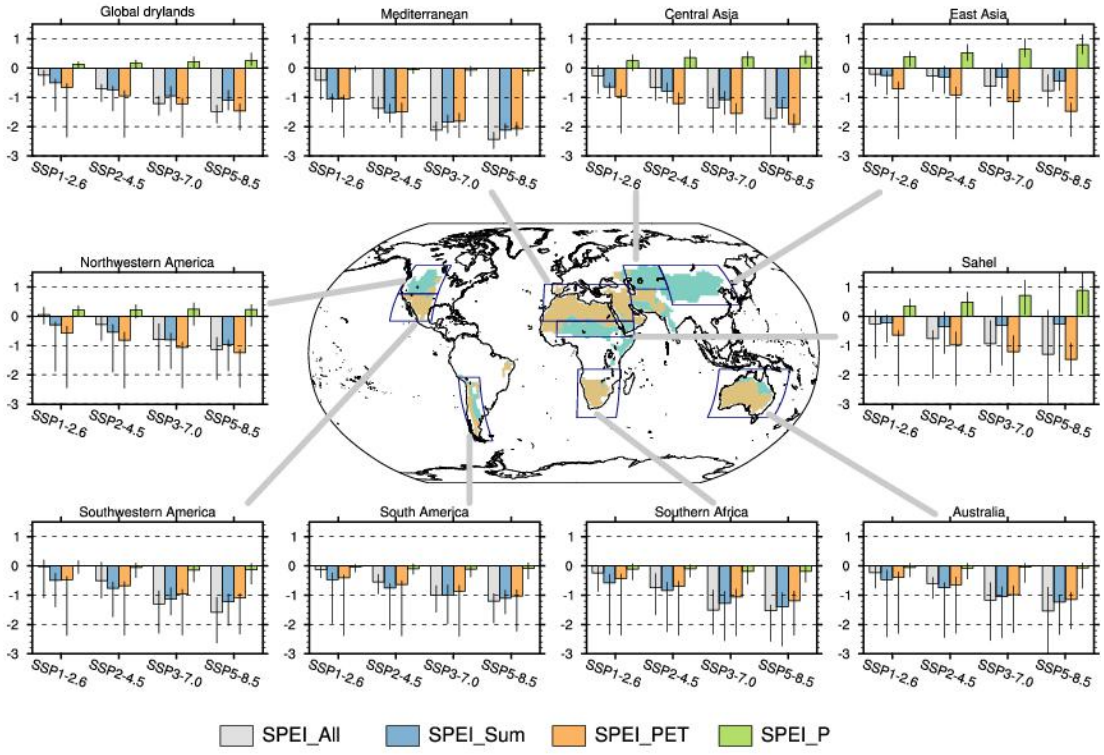

Figure 7. Multimodel median (bars) for trend (unit: /100yr) of SPEI_All (grey), SPEI_Sum (blue), SPEI_PET (orange) and SPEI_P (green) area-averaged over the global drylands and nine specific sub-drylands under SSP1-2.6, SSP2-4.5, SSP3-7.0, and SSP5-8.5 scenarios, respectively. The black lines indicate the interquartile ranges of the trend.

According to the formula (3–4), we obtain the contributions of PET and P to SPEI changes with respect to the 1960-1989 climatological drought condition. Figure 8 illustrates the multimodel medians for fractional contributions of PET and P across the global drylands and nine sub-drylands in the four periods under different scenarios, respectively. In the present day, contributions of PET and P to SPEI changes are almost equal across the global drylands. The contribution of PET (P) increases (decreases) relatively slowly with time under SSP1-2.6 and SSP2-4.5 scenarios, while rapidly under SSP3-7.0 and SSP5-8.5 scenarios. In addition, scenario discrepancies are relatively small in the near- and mid-term, but more evident in the long-term. For near-term projections, PET (P) contributes ~58% (~42%) under the four scenarios. In the mid-term, the fractional contribution of PET (P) further increases (declines) to ~61% (~39%) under the first three scenarios, while to ~68% (~32%) under SSP5-8.5

scenario. In the long-term, the fractional contribution of PET (P) is relatively stable [~65% (~35%)] under SSP1-2.6, but continue to increase (decrease) to ~72% (28%), ~80% (~20%), ~85% (~15%) under the other three scenarios, respectively. Regionally, the fractional contribution of PET (P) tends to increase more rapidly in the North Hemisphere than that in the South Hemisphere, especially under SSP3-7.0 and SSP5-8.5 scenarios. In particular, the contribution of PET (P) over the Mediterranean, central and East Asia drylands is much higher (lower) than the average across the global drylands. Under the two high scenarios, PET contributes to approximately or even more than 100% in the long-term due to the opposite roles of PET and P to drought changes. In the South Hemisphere, the contribution of PET (P) retains less than 70% (more than 30%) even under SSP5-8.5 because both PET and P are favorable of the intensifying drought condition.

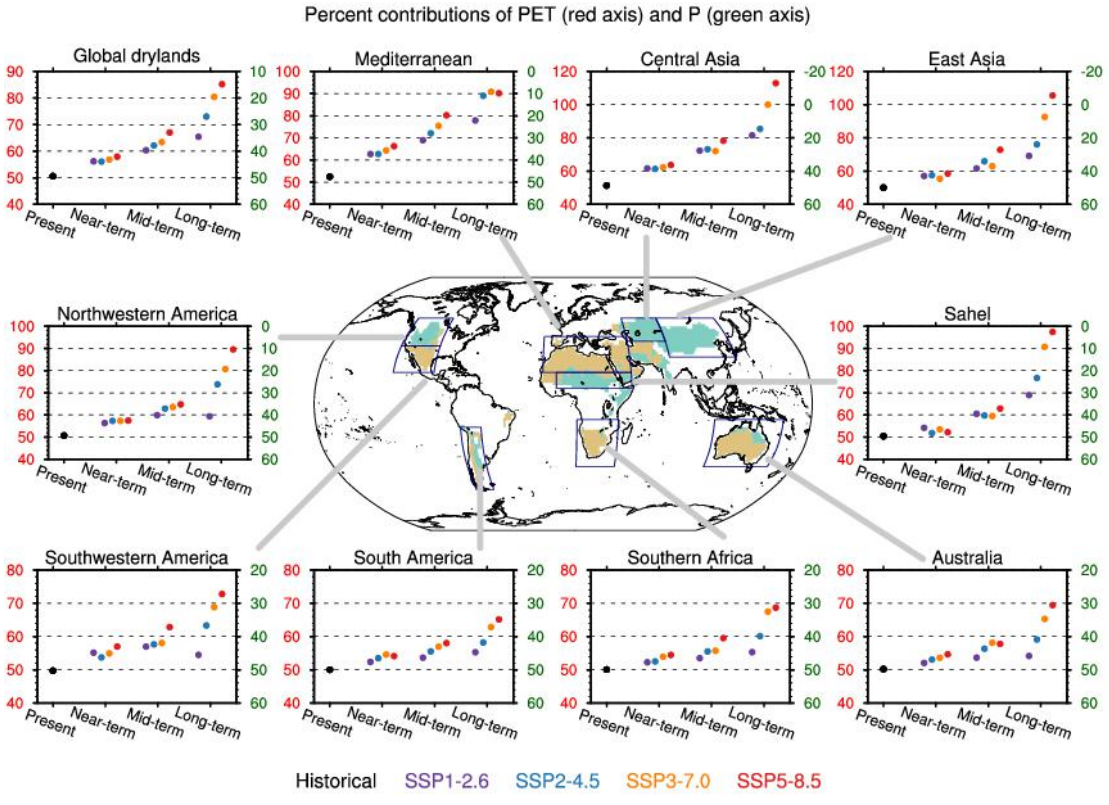

Figure 8. Multimodel medians for the fractional contributions (unit: %) of PET (left axis) and P (right axis) across global drylands and nine specific sub-drylands in the present day (1995–2014), near-term (2021–2040), mid-term (2041–2060), and long-term (2081–2100), estimated from the

historical (black) simulations and SSP1-2.6 (purple), SSP2-4.5 (blue), SSP3-7.0 (orange), and SSP5-8.5 (red) projections, respectively.

3.3 Future changes in drought impacts

To address detailed drought impacts and risks across global drylands for police-making, we investigate future changes in drought intensity, affected area fraction and occurrence. Given severe socio-economic impacts, we focus on the droughts above moderate level, i.e., SPEI_All<-1.0. Figure 9 provides the time series of area-averaged drought intensity, affected area fraction and occurrence across the global drylands during 1960–2100. All of the three metrics present a robust increasing in the 21st century, indicating droughts will occur more intensely, widespread and frequently across the global drylands. The drought intensity increases from ~-1.3 in the 20th century to ~-1.6, -1.8, -2.1 and -2.3 in the end of 21st century, the area fraction from ~20% to 38%, 40%, 58%, and 60%, and the occurrence from ~5 to 6.5, 7.5, 8.5 and 9.5 months per year, under SSP1-2.6, SSP2-4.5, SSP3-7.0, and SSP5-8.5 scenarios, respectively. The scenario inconsistencies are becoming more evident with time. Notably, the drought metrics tend to be stable and alleviative in the late 21st century under SSP1-2.6.

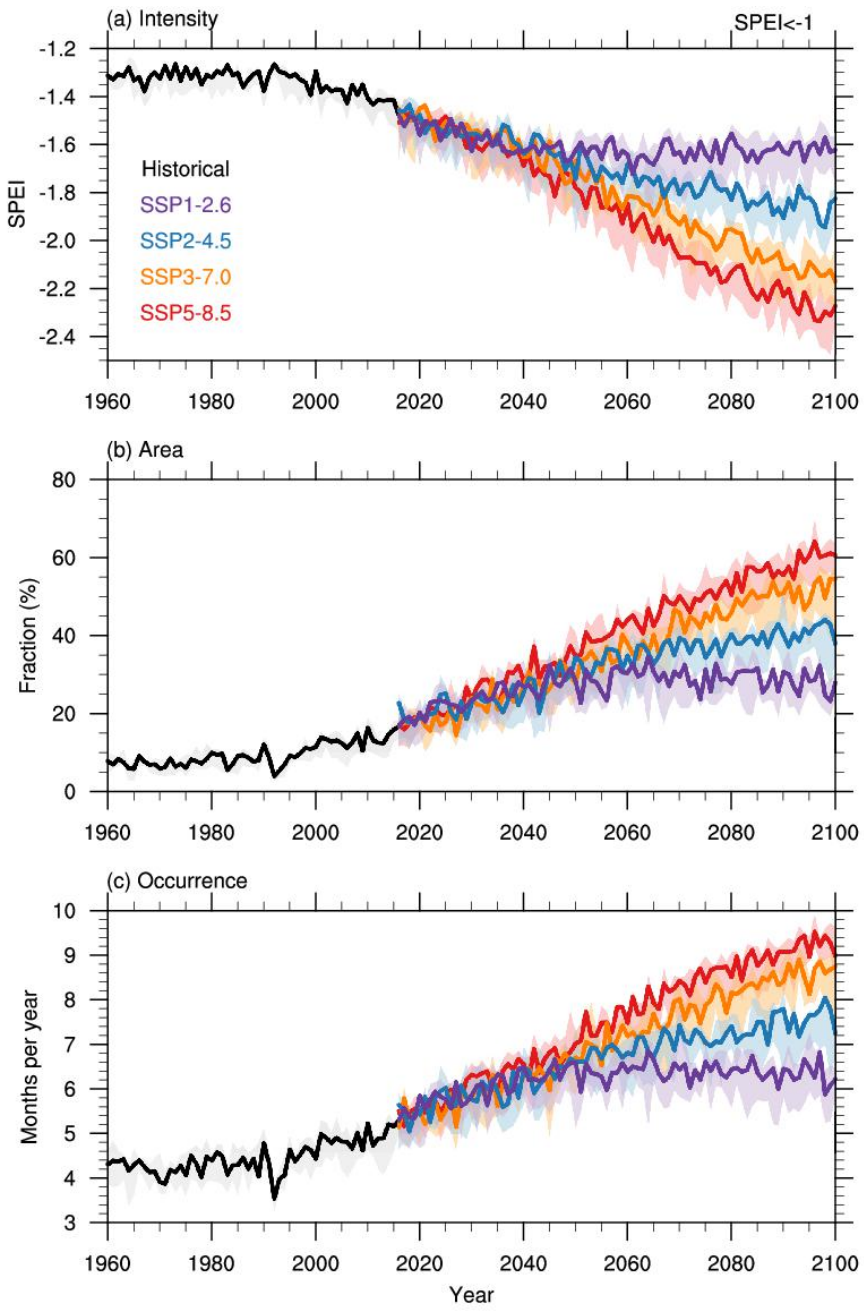

Figure 9. Time series of area-averaged drought (SPEI_All<-1.0) (a) intensity (b) affected area fraction (unit: %) and (c) occurrence (unit: months/yr) across the global drylands during 1960–2100. Historical (black), SSP1-2.6 (purple), SSP2-4.5 (blue), SSP3-7.0 (orange), and SSP5-8.5 (red) simulations are shown in median (lines) and interquartile ranges (shade).

Figure 10 further provides the probability density function (PDF) changes in drought affected area fraction and occurrence in the four periods under different scenarios, respectively. Obvious shift and flattening can be seen in the future PDFs

compared to that in the present day. Additionally, the future PDFs tend to be divergent among scenarios with time, indicating the increasing scenario uncertainties. In particular, we use the fractional area (21%) and occurrence (7.5 months/yr) of 1-in-20 years drought in the present day as thresholds to characterize extreme drought events. As to fractional area (occurrence), the probability reaches to 53.8–69.2% (27–29.1%) in the near-term, 84.6–95.8% (33–46.4%) in the mid-term, and 85.0–100% (33.2–75.3%) in the long-term under the four different scenarios, respectively. This suggests that the present-day 1-in-20-yr drought over global drylands would become dozens of times more common events, indicating that global drylands would be exposed to such severe droughts more widespread and long-lasting in the 21st century.

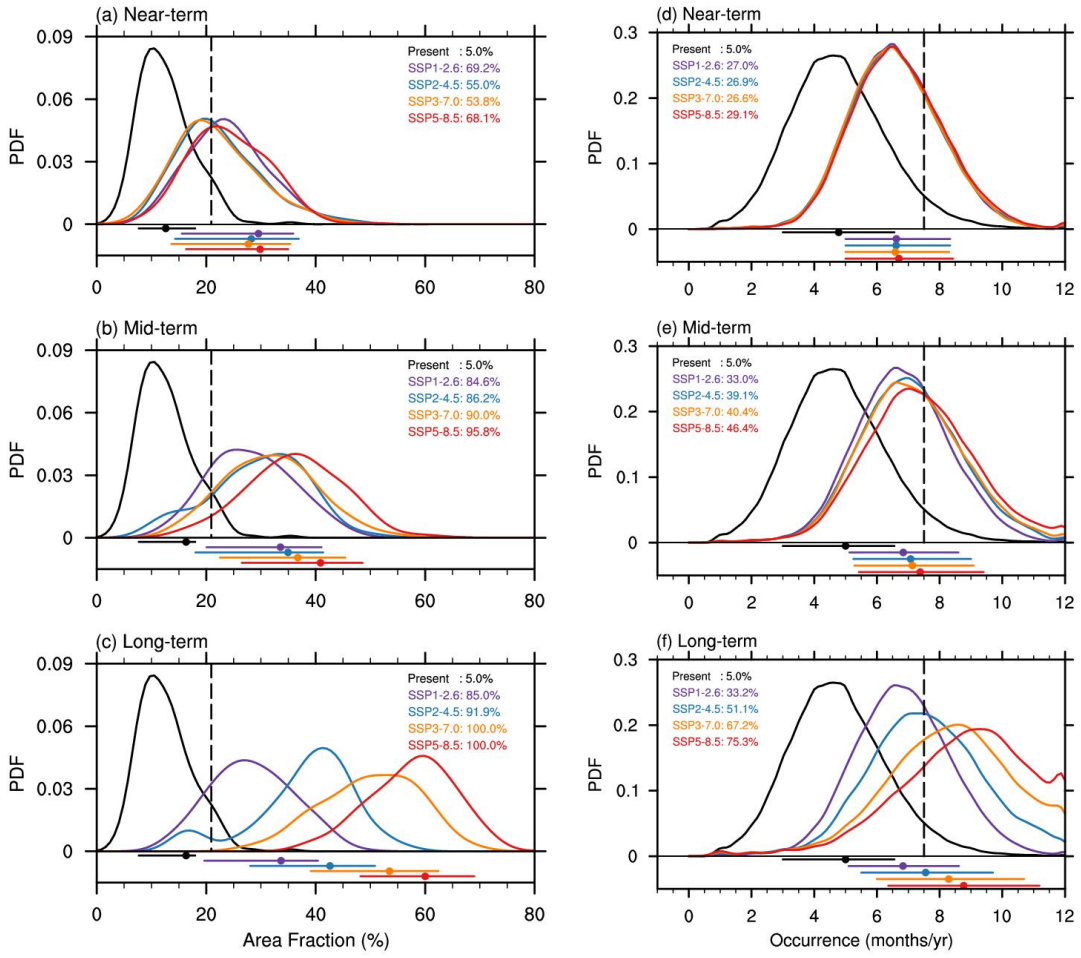

Figure 10. Probability density function (PDF) of drought affected area fraction (a–c, unit: %)

and occurrence (d–f, unit: months per year) across the global drylands in the near-term (2021–2040, a, d), mid-term (2041–2060, b, e) and long-term (2081–2100, c, f) periods under SSP1-2.6 (purple), SSP2-4.5 (blue), SSP3-7.0 (orange), and SSP5-8.5 (red) scenarios, compared with the present day (1995–2014) level from the historical simulations (black). In each panel, dots and horizontal lines in the bottom denote the average and the 10^{th} to 90^{th} range of PDFs, the black dash lines present the threshold of 1-in-20-yr drought event, and the numbers indicate future probabilities of such event.

4 Conclusions and discussions

In this study, we quantified the contributions of PET and P and investigated future drought changes throughout the global drylands in a warming climate, using historical simulations and projections under SSP1-2.6, SSP2-4.5, SSP3-7.0, SSP5-8.5 scenarios from 13 CMIP6 models. The conclusions are outlined as follows.

1) The hydroclimatic fields, including P, E, P-E and SM, present consistent trend distributions during 2015–2100 under the four scenarios. P-E and SM show a wetting over the regions where P and E increase robustly, including the East Asia, Middle East, Sahel and South Asia drylands. Likewise, P-E and SM tend to get drying over the regions where P and E decreases significantly or increases indistinctively, including the North America, South America, Mediterranean, central Asia, Southern Africa and Australia drylands.

2) Considering changes in both P and evaporative demand (PET), the drought index (SPEI) shows a widespread drying at a rate of -0.2 (-0.4, -0.2), -0.7 (-0.8, -0.6), -1.1 (-1.4, -1.0) and -1.4 (-1.7, -1.4) /100yr throughout the global drylands during 2015–2100 under the four scenarios, respectively. By partition the impacts of PET and P, we found that PET plays a critical role in drought intensification across global drylands.

3) In terms of the contributions of PET and P across the global drylands, they are approximately equal (~50%) to drought changes at present-day. In the 21st century, the impact of PET tends to be more evident with time and warming levels. Under the four scenarios, the contribution of PET (P) reaches ~58% (42%) and ~61% (~39%) in the near- and mid-term, respectively, with less scenario dependence. In the long-term, the contribution of PET (P) further increase to ~65% (~35%), ~72% (28%), ~80% (~20%), ~85% (~15%) under SSP1-2.6, SSP2-4.5, SSP3-7.0 and SSP5-8.5, respectively. In addition, the changes in contributions of PET and P show obvious regional dependence due to spatial discrepancies in P changes. The contribution of PET is larger in the North Hemisphere than that in the South Hemisphere. In particular, it approaches to nearly 100% in the long-term under SSP5-8.5 scenario over the regions where changes in PET and P offset each other, including the Mediterranean, central and East Asia drylands.

4) Three drought metrics area-averaged throughout the global drylands present a robust intensifying under the SSP3-7.0 and SSP5-8.5 scenarios, whereas tend to be stable and somewhat alleviative under the SSP1-2.6 and SSP2-4.5 scenarios in the late 21st century. The drought intensity is estimated to increase from ~-1.3 at present-day to ~-1.6, -1.8, -2.1 and -2.3, area fraction from ~20% to 38%, 40%, 58%, and 60%, and occurrence from ~5 to ~ 6.5, 7.5, 8.5 and 9.5 months per year under the SSP1-2.6, SSP2-4.5, SSP3-7.0, and SSP5-8.5 scenarios, respectively. Global drylands would be exposed to severe droughts like the present-day 1-in-20-yr events more widespread and long-lasting in the 21st century.

Furthermore, the following discussions should be noticed. First, we focus on the present drylands measured by the climatology of AI during 1960–2018, without considering the changes of dryland regions. It is undoubted that drylands would expand for more intense and frequent droughts in a warming climate (Fu & Feng, 2013; Huang et al., 2014). Secondly, because PET and P are not entirely independent,

SPEI_Sum is actually higher than SPEI_All to some extent (Cook et al., 2014). Here we use the first-order approximation of their relative contributions to drought changes. Finally, PET is overestimated derived from model outputs (Milly & Dunne, 2016; Greve et al., 2019), which maybe result in overestimating the contribution of PET to drought changes. Thus, reliable constraint methods for PET correction remain to be further investigated.

Acknowledgments

This study is supported by the Ministry of Science and Technology of China under Grant 2018YFA0606501 and National Natural Science Foundation of China under grant No. 42075037. We thank for the free open access datasets used in this study. The Climatic Research Unit gridded Time Series Version 4.03 (CRU TS v.4.03) was obtained from http://data.ceda.ac.uk/badc/cru/data/cru_ts/cru_ts_4.03. The CMIP6 simulations were obtained from https://esgf-node.llnl.gov/search/cmip6/. The authors declare no conflict of interest.

References

Ault, T. R. (2020). On the essentials of drought in a changing climate. *Science*, 368, 256-260. doi: 10.1126/science.abc4034

Barlow, M., Zaitchik, B., Paz, S., Black, E., Evans, J., & Hoell, A. (2016). A review of drought in the Middle East and Southwest Asia. *Journal of Climate,* 29, 8547-8574. https://doi.org/10.1175/JCLI-D-13-00692.1

Berg, A., Findell, K., Lintner, B., Giannini, A., Seneviratne, S. I., van den Hurk, B., et al. (2016). Land–atmosphere feedbacks amplify aridity increase over land under global warming. *Nature Climate Change*, 6, 869–874 https://doi.org/10.1038/nclimate3029

Burrell, A. L., Evans, J. P., & De Kauwe, M. G. (2020). Anthropogenic climate change has driven over 5 million km2 of drylands towards desertification, *Nature Communications*, **11**, 3853. https://doi.org/10.1038/s41467-020-17710-7

Cook, B. I., Smerdon, J. E., Seager, R., & Coats, S. (2014). Global warming and 21st century

drying. *Climate Dynamics*, **43**, 2607–2627. https://doi.org/10.1007/s00382-014-2075-y

Cook, B. I., Mankin, J. S., Marvel, K.,Williams, A. P., Smerdon, J. E., & Anchukaitis, K. J. (2020). Twenty-first century drought projections in the CMIP6 forcing scenarios. *Earth's Future*, 8, e2019EF001461. https://doi. org/10.1029/2019EF001461

Dai, A. (2013). Increasing drought under global warming in observations and models. *Nature Climate Change*, **3**, 52-58. https://doi.org/10.1038/NCLIMATE1633

Dai, A. (2021). Hydroclimatic trends during 1950-2018 over global land. *Climate Dynamics*, https://link.springer.com/article/10.1007/s00382-021-05684-1.

Dai, A., Zhao, T., & Chen, J. (2018). Climate change and drought: A precipitation and evaporation perspective. *Current Climate Change Reports*, **4**, 301 – 312. https:/ /doi.org/10.1007/s40641-018-0101-6

Dai, A., & Zhao, T. (2017). Uncertainties in historical changes and future projections of drought. Part I: estimates of historical drought changes. *Climatic Change*, 144, 519-533. DOI 10.1007/s10584-016-1705-2

D'Odorico, P., & Bhattachan, A. (2012). Hydrologic variability in dryland regions: impacts on ecosystem dynamics and food security. *Philosophical Transactions of the Royal Society*, 367, 3145-3157. https://doi.org/10.1098/rstb.2012.0016

Eyring, V., Bony, S., Meehl, G. A., Senior, C. A., Stevens, B., Stouffer, R. J., et al. (2016). Overview of the Coupled Model Intercomparison Project Phase 6 (CMIP6) experimental design and organization. *Geoscientific Model Development*, **9**, 1937–1958. https://doi.org/10.5194/gmd-9-1937-2016

Feng, S., & Fu, Q. (2013). Expansion of global drylands under a warming climate. *Atmospheric Chemistry & Physics Discussions*, **13**, 14637 – 14665. doi:10.5194/acpd-13-14637-2013

Fragaszy, S. R., Jedd, T., Wall, N., Knutson, C., Fraj, M. B., Bergaoui, K., et al. (2020). Drought monitoring in the Middle East and North Africa (MENA) region: Participatory engagement to inform early warning systems, *Bulletin of the American Meteorological Society*, 101(7), E1148-E1173. https://doi.org/10.1175/BAMS-D-18-0084.1

Fu, Q., & Feng, S. (2014). Responses of terrestrial aridity to global warming, *Journal of*

Geophysical Research Atmospheres, **119**, 7863–7875, doi:10.1002/2014JD021608.

Gill, J. C., & Malamud, B. D. (2014). Reviewing and visualizing the interactions of natural hazards. *Reviews of Geophysics*, 52, 680-722, https://doi.org/10.1002/2013RG000445

Greve, P., Roderick M. L., Ukkola A. M., & Wada, Y. (2019). The aridity Index under global warming. *Environmental Research Letters*, **14**, 124006. https://doi.org/10.1088/1748-9326/ab5046

Hari, V., Rakovec, O., Markonis, Y., Hanel, M., & Kumar, R. (2020). Increased future occurrences of the exceptional 2018-2019 Central European drought under global warming. *Scientific Reports*, **10**,12207. https://doi.org/10.1038/s41598-020-68872-9

Harris, I., Osborn, T. J., Jones, P., & Lister, D. (2020). Version 4 of the CRU TS monthly high-resolution gridded multivariate climate dataset. *Scientific Data*, **7**, 109 | https://doi.org/10.1038/s41597-020-0453-3

Huang, J., Guan, X., & Ji, F. (2012). Enhanced cold-season warming in semi-arid regions. *Atmospheric Chemistry and Physics*, **12**, 5391–5398. DOI: 10.5194/acpd-12-4627-2012

Huang, J., Yu, H., Guan, X., Wang, G. & Guo, R. (2015). Accelerated dryland expansion under climate change. Nature Climate Change, **26**, 1-7. DOI: 10.1038/NCLIMATE2837

Huang, J., Li, Y., Fu, C., Chen, F., Fu, Q., Dai, A., et al. (2017a). Dryland climate change: Recent progress and challenges. *Reviews of Geophysics*, **55**, 719–778. doi:10.1002/2016RG000550.

Huang, J., Yu, H., Dai, A., Wei, Y., & Kang, L. (2017b). Drylands face potential threat under 2℃ global warming target. *Nature Climate Change*, **7**, 417-422. DOI: 10.1038/NCLIMATE3275

Huang, J., Zhang, G., Zhang, Y., Guan, X., Wei, Y., & Guo, R. (2020). Global desertification vulnerability to climate change and human activities. *Land Degradation & Development*, **31**, 1-12. DOI: 10.1002/ldr.3556

Hulme, M. (1996). Recent climatic change in the world's drylands, *Geophysical Research Letters*, **23**, 61–64. DOI: 10.1029/95GL03586

Ji, F., Wu, Z., Huang, J., & Chassignet, E. P. (2014). Evolution of land surface air temperature trend. *Nature Climate Change*, **4**, DOI: 10.1038/NCLIMATE2223

556 Lehner, F., Coats, S., Stocker, T. F., Pendergrass, A. G., Sanderson, B. M., Raible, C. C., et al.
557 (2017). Projected drought risk in 1.5°C and 2°C warmer climates, *Geophysical Research*
558 *Letters*, **44**, 7419–7428, https://doi.org/10.1002/2017GL074117
559 Liu, Y., & Chen, J. (2021). Future global socioeconomic risk to droughts based on estimates of
560 hazard, exposure, and vulnerability in a changing climate. *Science of the Total Environment*,
561 751, 142159. https://doi.org/10.1016/j.scitotenv.2020.142159
562 Mannava, V.K., Sivakumar, R. L., Ramasamy, S., et al. (2013). Climate Change and Food Security
563 in West Asia and North Africa [M]. Springer.
564 Mankin, J. S., Seager, R., Smerdon, J. E., Cook, B. I., & Williams, A. P. (2019). Mid-latitude
565 freshwater availability reduced by projected vegetation responses to climate change. *Nature*
566 *Geoscience*, **12**, 983–988. https://doi.org/10.1038/s41561-019-0480-x
567 Miao, L., Li, S., Zhang, F., Chen, T., Shan, Y., & Zhang, Y. (2020). Future drought in the dry lands
568 of Asia under the 1.5 and 2.0 °C warming scenarios. *Earth's Future*, **8**, e2019EF001337.
569 https://doi.org/10.1029/2019EF001337
570 Middleton, N. J. & Thomas, D. S. G. (1992). UNEP: World atlas of desertification, Edward Arnold,
571 Sevenoaks.
572 Milly, P. C. D., & Dunne, K. A. (2016). Potential evapotranspiration and continental drying.
573 *Nature Climate Change*, **6**, 946-949. DOI: 10.1038/NCLIMATE3046
574 Monteith, J. I. L. (1965). Evaporation and Environment. *Symposia of the Society for Experimental*
575 *Biology*, **19**, 205–234.
576 O'Neill, B. C., Tebaldi, C., van Vuuren, D. P., Eyring, V., Friedlingstein, P., Hurtt, G., et al. (2016).
577 The scenario model intercomparison project (ScenarioMIP) for CMIP6. *Geoscientific Model*
578 *Development*, **9**, 3461−3482, https://doi.org/10.5194/gmd-9-3461-2016.
579 O'Neill, B. C., Kriegler, E., Ebi, K. L., Kemp-Benedict, E., Riahi, K., Rothman, D. S., et al.
580 (2017). The roads ahead: narratives for shared socioeconomic pathways describing world
581 futures in the 21st century. *Global Environmental. Change*, **42**, 169–180.
582 http://dx.doi.org/10.1016/j.gloenvcha.2015.01.004
583 Penman, H. L. (1948). Natural evaporation from open water, bare soil and grass. Proceedings of

584 The Royal Society A, **193**, 120–145. DOI：10.1098/rspa.1948.0037

585 Scheff, J., & Frierson, D. M. W. (2015). Terrestrial Aridity and Its Response to Greenhouse
586 Warming across CMIP5 Climate Models. *Journal of Climate*, **15**, 5583-5600. DOI:
587 10.1175/JCLI-D-14-00480.1

588 Schlaepfer, D., Bradford, J., Lauenroth, W., Munson, S., M., Tietjen, B., Hall, S. A., et al. (2017).
589 Climate change reduces extent of temperate drylands and intensifies drought in deep soils.
590 *Nature Communications*, **8**, 14196. https://doi.org/10.1038/ncomms14196

591 Sherwood, S. & Fu, Q. (2014). A drier future? Science, 343, 737–739. DOI:
592 10.1126/science.1247620

593 Spinoni, J., Barbosa, P., Bucchignani, E., Cassano, J., Cavazos, T., Christensen, J. H., et al. (2020).
594 Future global meteorological drought hot spots: A study based on CORDEX data. *Journal of*
595 *Climate*, **33**, 3635-3661. DOI: 10.1175/JCLI-D-19-0084.1

596 Takeshima, A., Kim, H., Shiogama, H., Lierhammer, L., Scinocca, J. F., Seland, Ø., et al. (2020).
597 Global aridity changes due to differences in surface energy and water balance between 1.5 °C
598 and 2 °C warming. *Environmental Research Letters*, **15**, 0940a7.
599 https://doi.org/10.1088/1748-9326/ab9db3

600 Trenberth, K. E, Dai, A., van der Schrier, G., Jones, P. D., Barichivich, J., Briffa, K. R., et al.
601 (2014). Global warming and changes in drought. *Nature Climate Change*, **4**, 17-22.
602 https://doi.org/10.1038/NCLIMATE2067

603 Ukkola, A. M., De Kauwe, M. G., Roderick, M. L., Abramowitz, G., & Pitman, A. J. (2020).
604 Robust future changes in meteorological drought in CMIP6 projections despite uncertainty in
605 precipitation. *Geophysical Research Letters*, **46**, e2020GL087820. https://doi.
606 org/10.1029/2020GL087820

607 United Nations Development Programme (UNDP). (2014), Environment and energy, drylands
608 development centre, where we work, Accessed 19 Jan 2014.

609 Vicente-Serrano, S. M., Beguería, S. & López-Moreno, J. I. (2010). A multiscalar drought index
610 sensitive to global warming: the standardized precipitation evapotranspiration index. *Journal*
611 *of Climate*, **23**, 1696 – 1718. DOI:10.1175/2009JCLI2909.1

612 Vicente-Serrano, S. M., Beguería, S. & López-Moreno, J. I. (2012). Performance of Drought
613 Indices for Ecological, Agricultural, and Hydrological Applications. *Earth Interactions*, **16**,
614 1-27. DOI: 10.1175/2012EI000434.1
615 Vicente-Serrano, S. M., Quiring S. M., Peña-Gallardo M., Yuan S., & Domínguez-Castro F. (2020).
616 A review of environmental droughts: Increased risk under global warming? *Earth-Science*
617 *Reviews*, 201, 102953. https://doi.org/10.1016/j.earscirev.2019.102953
618 Wei, Y., Yu, H., Huang, J., Zhou, T., Zhang, M., & Ren, Y. (2019). Drylands climate response to
619 transient and stabilized 2 °C and 1.5 °C global warming targets. *Climate Dynamics*, **53**,
620 2375–2389. https://doi.org/10.1007/s00382-019-04860-8
621 White, R. P., & Nackoney, J. (2003). Drylands, People and Ecosystem Goods and Services, World
622 Resources Institute, Washington.
623 Xie, R. H., & Wang, A. H. (2020). Comparison of ten potential evapotranspiration models and
624 their attribution analyses for ten Chinese drainage basins. *Advances in Atmospheric Sciences*,
625 **37**, 959−974. https://doi.org/10.1007/s00376-020-2105-0.
626 Yao, J., Liu, H., Huang, J., Gao, Z., Wang, G., Li, D., et al. (2020). Accelerated dryland expansion
627 regulates future variability in dryland gross primary production. *Nature Communications*, **11**,
628 1665. https://doi.org/10.1038/s41467-020-15515-2
629 Zhang, X., Tang, Q., Zhang, X., & Lettenmaier, D. P. (2014). Runoff sensitivity to global mean
630 temperature change in the CMIP5 Models. *Geophysical Research Letters*, **41**, 5492–5498.
631 https://doi.org/10.1002/2014GL060382
632 Zhao, T., & Dai, A. (2017). Uncertainties in historical changes and future projections of drought.
633 Part II: model-simulated historical and future drought changes. *Climatic Change*, **144**,
634 535-548. DOI 10.1007/s10584-016-1742-x
635 Zhou, S., Zhang, Y., Williams, A. P., & Gentine, P. (2019). Projected increases in intensity,
636 frequency, and terrestrial carbon costs of compound drought and aridity events. *Science*
637 *Advances*, **5**, eaau5740. DOI: 10.1126/sciadv.aau5740
638 Zhou, S., Williams, A.P., Lintner, B.R., Berg, A. M., Zhang, Y., Keenan T. F., et al. (2021). Soil
639 moisture–atmosphere feedbacks mitigate declining water availability in drylands. *Nature*
640 *Climate Change,* **11**, 38–44. https://doi.org/10.1038/s41558-020-00945-z

641 Zotarelli, L., Dukes, M. D., Migliaccio, K. W., & Morgan, A. K. T. (2013). Step by Step
642 Calculation of the Penman-Monteith Evapotranspiration (FAO-56 Method) www:
643 http://edis.ifas.ufl.edu/pdffiles/ae/ae45900.pdf